

Microscopic spin-wave theory for yttrium-iron garnet films

Andreas Kiesel, Francesca Sauli, Lorenz Bartosch, and Peter Kopietz

Institut für Theoretische Physik, Universität Frankfurt, Max-von-Laue-Strasse 1, 60438 Frankfurt, Germany

August 25, 2009

Abstract. Motivated by recent experiments on thin films of the ferromagnetic insulator yttrium-iron garnet (YIG), we have developed an efficient microscopic approach to calculate the spin-wave spectra of these systems. We model the experimentally relevant magnon band of YIG using an effective quantum Heisenberg model on a cubic lattice with ferromagnetic nearest neighbour exchange and long-range dipole-dipole interactions. After a bosonization of the spin degrees of freedom via a Holstein-Primakoff transformation and a truncation at quadratic order in the bosons, we obtain the spin-wave spectra for experimentally relevant parameters without further approximation by numerical diagonalization, using efficient Ewald summation techniques to carry out the dipolar sums. We compare our numerical results with two different analytic approximations and with predictions based on the phenomenological Landau-Lifshitz equation.

PACS. 75.10.Jm Quantized spin models { 75.30.Ds Spin waves { 05.30.Jp Boson systems

1 Introduction

In a recent series of experiments [1,2,3,4,5] Demokritov and co-workers discovered strong correlations of highly occupied magnon states in thin films of the magnetic insulator yttrium-iron garnet (YIG) with stoichiometric formula $Y_3Fe_2(FeO_4)_3$. They suggested an interpretation of their results in terms of Bose-Einstein condensation of magnons at room temperature. For a proper interpretation of these experiments, a peculiar feature of the energy dispersion E_k of the relevant magnon band in finite YIG films is important: due to a subtle interplay between finite-size effects, short-range exchange interactions, and long-range dipole-dipole interactions, E_k exhibits a local minimum at a finite wave-vector k_{min} , for a certain range of orientations of the external magnetic field H_e relative to the sample. The existence of such a dispersion minimum has been predicted by Kalinikos and Slavin [6,7] within a phenomenological approach based on the Landau-Lifshitz equation. Unfortunately, such a phenomenological approach does not provide a microscopic understanding of correlation effects, which might be important to explain some aspects of experiments probing the non-equilibrium behaviour of the magnon gas in YIG [1,2,3,4,5,8,9,10,11]. This has motivated us to study this problem within the framework of the usual $1/S$ -expansion for ordered quantum spin systems, which is based on the bosonization of an effective microscopic Heisenberg model using either the Holstein-Primakoff [12] or the Dyson-Maleev transformation [13, 14], and the subsequent classification of the interaction processes in powers of the small parameter $1/S$.

The $1/S$ -expansion has been extremely successful to understand spin-wave interactions in ordered magnets [15, 16]. Previously, several authors have used this approach

to calculate spin-wave spectra in ultrathin ferromagnetic films with exchange and dipole-dipole interactions [17,18, 19,20]. Moreover, interaction effects such as energy shifts and damping of spin-waves in thin films have also been calculated within the $1/S$ -expansion [21,22]. However, in order to apply this approach to realistic models for experimentally relevant YIG films with a thickness of a few microns (corresponding to a few thousand lattice spacings), one has to evaluate numerically rather large dipolar sums [23] to set up the secular matrix whose eigenvalues determine the magnon modes, see Eq. (18) below. We use here an efficient Ewald summation technique [24] to carry out these summations, which enables us to calculate the spin-wave dispersions of realistic YIG films. Given our numerical results, we can assess the validity of various analytical approximations such as the uniform mode approximation [6,20,25] and the lowest eigenmode approximation.

The rest of this paper is organized as follows: In Sec. 2 we introduce the effective Heisenberg model which we shall use to describe the experimentally relevant magnon band in YIG. We set up the $1/S$ -expansion and derive the secular equation which determines the magnon dispersion. In Sec. 3 we present our results for the magnon spectra of YIG. We first discuss our numerical results, which are obtained by evaluating the roots of the secular determinant without further approximation, using the Ewald summation technique described in the appendix to evaluate the necessary dipolar sums. We then discuss in Secs. 3.2 and 3.3 two approximate analytical methods for obtaining the dispersion of the lowest magnon band. A comparison with our numerical results allows us to estimate the accuracy

of these approximations. Finally, in Sec. 4 we present our conclusions and give an outlook for further research.

2 Effective Hamiltonian for YIG films

Experimental and theoretical research on YIG has a long history, as reviewed, for example, in Ref. [26]. Some distinct advantages of YIG are that this material can be grown in very pure crystals and has a very narrow ferromagnetic resonance line, indicating very low spin-wave damping. Actually, YIG is a ferrimagnet at accessible magnetic fields and has a rather complicated crystal structure with space group Ia3d (see Refs. [26,27]) and 20 magnetic ions in the primitive cell. Fortunately, on the energy scales relevant to experiments [1,2,3,4,5,8,9,10,11] only the lowest magnon band is important, so that we can describe the physical properties of YIG at room temperature in terms of an effective spin S quantum Heisenberg ferromagnet on a cubic lattice with lattice spacing [27]

$$a = 12.376 \text{ \AA} ; \quad (1)$$

The effective Hamiltonian contains both exchange and dipole-dipole interactions,

$$\hat{H} = \frac{1}{2} \sum_{ij} J_{ij} S_i \cdot S_j + \mu_B H_e \sum_i S_i^z + \frac{1}{2} \sum_{ij, i \neq j} \frac{2\hbar}{R_{ij}^3} 3(S_i \cdot \hat{R}_{ij})(S_j \cdot \hat{R}_{ij}) - S_i \cdot \hat{S}_j ; \quad (2)$$

where the sums are over the sites R_i of the lattice and $\hat{R}_{ij} = R_{ij}/R_{ij}$ are unit vectors in the direction of $R_{ij} = R_i - R_j = x_{ij}e_x + y_{ij}e_y + z_{ij}e_z$. Here, μ_B is the magnetic moment associated with the spins, where g is the effective g -factor and $\mu_B = e\hbar/(2mc)$ is the Bohr magneton. The exchange energies $J_{ij} = J(R_i - R_j)$ decay rapidly with distance, so that it is sufficient to include only nearest neighbour exchange couplings in Eq. (2), setting $J_{ij} = J$ if R_i and R_j are nearest neighbours, and $J_{ij} = 0$ otherwise. Note that we neglect surface anisotropies which might be present in experiments, especially at the surface of the film which is attached to the substrate. Experimentally, the material YIG is characterized by its saturation magnetization [28]

$$4 M_S = 1750 G ; \quad (3)$$

and the exchange stiffness \mathcal{A}_{ex} of long-wavelength spin-waves [29],

$$\frac{\mathcal{A}_{ex}}{a} = \frac{J S a^2}{2} = 5.17 \cdot 10^{13} \text{ Oe m}^2 ; \quad (4)$$

If we arbitrarily set the effective g -factor equal to two [28] so that $\mu_B = 2 \mu_B$, we obtain from Eqs. (3) and (4) for the effective spin

$$S = \frac{M_S a^3}{2 \mu_B} = 14.2 ; \quad (5)$$

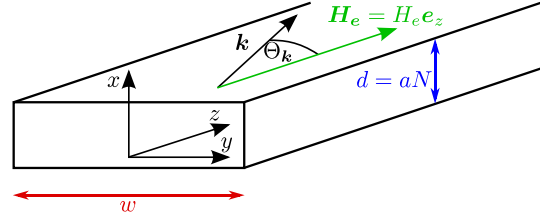


Fig. 1. (Color online) Orientation of our coordinate system for an infinitely long stripe of width w and thickness d . We assume that the external magnetic field $H_e e_z$ is parallel to the long axis (which we call the z -axis) of the stripe.

and for the nearest neighbour exchange coupling

$$J = 1.29 K ; \quad (6)$$

Our above estimates for S and J differ slightly from the values given in Ref. [30]. Note that the effective spin $S = 14.2$ is quite large, so that an expansion in powers of $1/S$ is justified. Introducing the dipolar tensor $D_{ij} = D(R_i - R_j)$,

$$D_{ij} = (1 - \delta_{ij}) \frac{2\hbar}{R_{ij}^3} 3\hat{R}_{ij} \hat{R}_{ij}^T - \frac{1}{R_{ij}^3} ; \quad (7)$$

we can write our effective Hamiltonian (2) in the compact form

$$\hat{H} = \frac{1}{2} \sum_{ij} J_{ij} S_i \cdot S_j + \sum_i h_i S_i^z + \sum_{ij} D_{ij} S_i \cdot S_j ; \quad (8)$$

where the z -axis of our coordinate system points into the direction defined by the magnetic field H_e and we have introduced the associated Zeeman energy,

$$h_i = \mu_B H_e ; \quad (9)$$

We have thus related the set of parameters $a; S; J; h$ appearing in our effective Hamiltonian to experimentally measurable quantities.

To proceed, we restrict ourselves to the description of an infinitely long stripe of width w and thickness $d = Na$, consisting of N layers. For the stripe geometry shown in Fig. 1 where the magnetic field points in any direction parallel to the stripe the classical groundstate is a saturated ferromagnet. Therefore we can expand the Hamiltonian in terms of bosonic operators describing fluctuations around the classical groundstate, using either the Holstein-Primakoff or Dyson-Maleev transformation [15, 16]. The resulting bosonized spin Hamiltonian is of the form

$$\hat{H} = H_0 + \sum_{n=2}^{\infty} \hat{H}_n ; \quad (10)$$

It turns out that Holstein-Primakoff and Dyson-Maleev transformations give different results for \hat{H}_n with $n \geq 4$,

but the expressions for \hat{H}_2 and \hat{H}_3 are identical in both transformations. The classical ground state energy is

$$H_0 = \frac{S^2}{2} \sum_{ij} J_{ij} + D_{ij}^{zz} + \frac{2J_{ij}}{2S} \frac{D_{ij}^{zz}}{2S}; \quad (11)$$

and the quadratic part of the Hamiltonian reads

$$\hat{H}_2 = \sum_{ij} A_{ij} b_i^y b_j + \frac{B_{ij}}{2} b_i b_j + b_i^y b_j^y; \quad (12)$$

with

$$A_{ij} = \sum_{in} j_{ij} h + S \sum_{in} J_{in} J_{ij} + S \sum_{in} D_{in}^{zz} \frac{D_{ij}^{xx} + D_{ij}^{yy}}{2}; \quad (13a)$$

$$B_{ij} = \frac{S}{2} D_{ij}^{xx} - 2iD_{ij}^{xy} - D_{ij}^{yy}; \quad (13b)$$

Since $\hat{H}_n = S^2 = 0$ ($l = S^{n=2}$) and the effective S is large, we expect accurate results even if we only keep the first two terms. In order to proceed we have to keep in mind that a stripe with thickness d and width w is obviously not translationally invariant, so that we cannot simply use a full Fourier transform to diagonalize the Hamiltonian. Because in the experimentally studied samples [1, 2, 3, 4, 5, 8, 9, 10, 11] the width w of the stripe is much larger than the thickness d , we can assume that w is practically infinite, so that our system can be considered to have discrete translational invariance in the y - and z -directions. We may then partially diagonalize \hat{H}_2 in Eq. (12) by performing a partial Fourier transformation in the yz -plane. Setting $R_i = (\mathbf{x}_i; r_i)$ with $r_i = (y_i; z_i)$, and introducing the two-dimensional wave-vector $\mathbf{k} = (k_y; k_z)$ in the yz -plane, we expand

$$b_i = \frac{1}{\sqrt{N_y N_z}} \sum_{\mathbf{k}} e^{i\mathbf{k} \cdot \mathbf{r}_i} b_{\mathbf{k}}(\mathbf{x}_i); \quad (14)$$

where N_y and N_z is the number of lattice sites in y and z direction. Our Hamiltonian \hat{H}_2 in Eq. (12) takes then the form

$$\begin{aligned} \hat{H}_2 = & \sum_{\mathbf{k}} \sum_{\mathbf{x}_i, \mathbf{x}_j} A_{\mathbf{k}}(\mathbf{x}_{ij}) b_{\mathbf{k}}^y(\mathbf{x}_i) b_{\mathbf{k}}(\mathbf{x}_j) \\ & + \frac{B_{\mathbf{k}}(\mathbf{x}_{ij})}{2} b_{\mathbf{k}}(\mathbf{x}_i) b_{\mathbf{k}}(\mathbf{x}_j) \\ & + \frac{B_{\mathbf{k}}(\mathbf{x}_{ij})}{2} b_{\mathbf{k}}^y(\mathbf{x}_i) b_{\mathbf{k}}^y(\mathbf{x}_j); \end{aligned} \quad (15)$$

with the amplitude factors [21, 22]

$$\begin{aligned} A_{\mathbf{k}}(\mathbf{x}_{ij}) &= \sum_{\mathbf{r}} e^{i\mathbf{k} \cdot \mathbf{r}} A(\mathbf{x}_i, \mathbf{x}_j; \mathbf{r}); \\ &= S J_{\mathbf{k}}(\mathbf{x}_{ij}) + \sum_{in} D_{in}^{zz}(\mathbf{x}_{in}) \\ & \quad \frac{S}{2} D_{\mathbf{k}}^{xx}(\mathbf{x}_{ij}) + D_{\mathbf{k}}^{yy}(\mathbf{x}_{ij}); \end{aligned} \quad (16a)$$

$$\begin{aligned} B_{\mathbf{k}}(\mathbf{x}_{ij}) &= \sum_{\mathbf{r}} e^{i\mathbf{k} \cdot \mathbf{r}} B(\mathbf{x}_i, \mathbf{x}_j; \mathbf{r}) \\ &= \frac{S}{2} D_{\mathbf{k}}^{xx}(\mathbf{x}_{ij}) - 2iD_{\mathbf{k}}^{xy}(\mathbf{x}_{ij}) - D_{\mathbf{k}}^{yy}(\mathbf{x}_{ij}); \end{aligned} \quad (16b)$$

and the exchange matrix

$$J_{\mathbf{k}}(\mathbf{x}_{ij}) = J_{ij} \frac{1}{2} (\cos(k_y a) + \cos(k_z a)) \quad (17)$$

3 Spin-wave spectra of YIG

3.1 Numerical approach

If the lattice has N sites in the x -direction, then for fixed two-dimensional wave-vector \mathbf{k} there are N allowed magnon energies $E_{n\mathbf{k}}$, $n = 0; \dots; N-1$, which are given by the positive zeros of the secular determinant

$$\det \begin{pmatrix} E_{\mathbf{k}} & A_{\mathbf{k}} & B_{\mathbf{k}} \\ & B_{\mathbf{k}} & E_{\mathbf{k}} \\ & & A_{\mathbf{k}} \end{pmatrix} = 0; \quad (18)$$

Here, the $N \times N$ matrices $A_{\mathbf{k}}$ and $B_{\mathbf{k}}$ are defined by

$$A_{\mathbf{k}} l_{ij} = A_{\mathbf{k}}(\mathbf{x}_{ij}); \quad (19a)$$

$$B_{\mathbf{k}} l_{ij} = B_{\mathbf{k}}(\mathbf{x}_{ij}); \quad (19b)$$

where $l_{ij}; j = 1 \dots N$ label now the lattice sites in the x -direction. The condition (18) follows simply from the fact that the magnon energies can be identified with the poles of the propagators of the Gaussian field theory defined by the quadratic Hamiltonian (15). Note that for $N = 1$ the condition (18) correctly reduces to the diagonalization of the Hamiltonian (15) via Bogoliubov transformation. To obtain the complete magnon spectrum of the thin film ferromagnet we have to calculate the dipolar matrices in Eq. (16) which leads to the calculation of the following dipolar sums for fixed \mathbf{x}_{ij} ,

$$\begin{aligned} D_{\mathbf{k}}(\mathbf{x}_{ij}) &= \sum_{\mathbf{r}} e^{i\mathbf{k} \cdot \mathbf{r}} D_{ij} \\ &= \sum_{\mathbf{r}_{ij}; z_{ij}} e^{i(k_y y_{ij} + k_z z_{ij})} \\ & \quad \frac{3r_{ij} r_{ij}}{(\mathbf{x}_{ij}^2 + y_{ij}^2 + z_{ij}^2)^{3=2}} - \frac{3r_{ij} r_{ij}}{(\mathbf{x}_{ij}^2 + y_{ij}^2 + z_{ij}^2)^{5=2}}; \end{aligned} \quad (20)$$

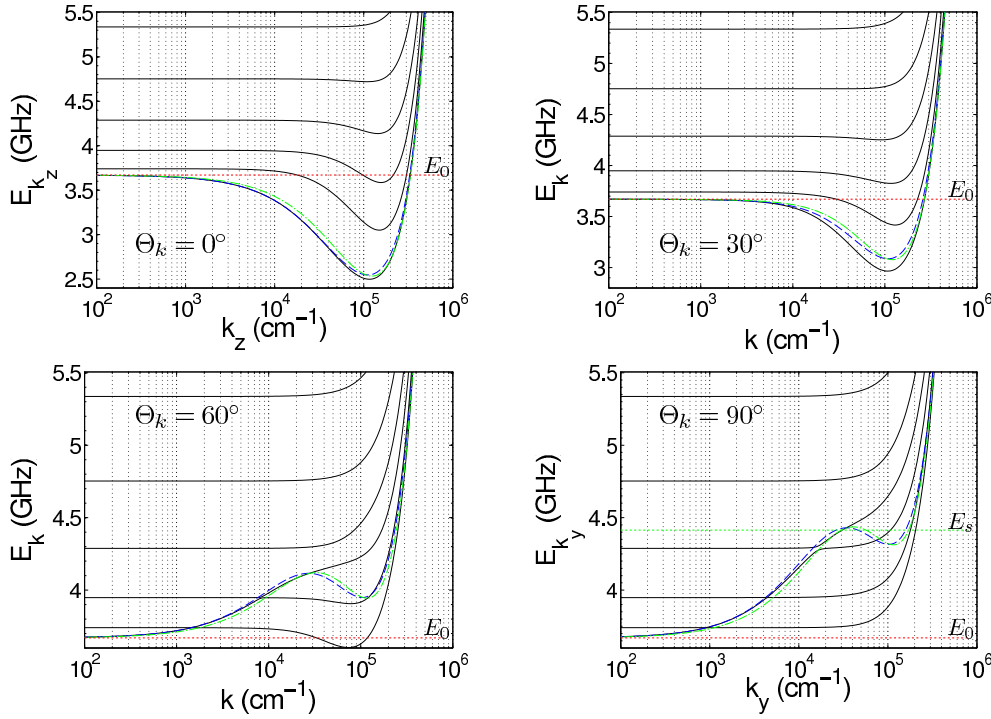


Fig. 2. (Color online) Spin-wave dispersion of a YIG film with thickness $d = 400 \text{ \AA} = 0.495 \text{ \mu m}$ in a magnetic field of 700 Oe for wave-vectors in the plane of the film and for different propagation angles $\Theta_k = 0; 30; 60; 90$ relative to the magnetic field (from top left to bottom right). The black solid curves represent the results from the numerical approach for the lowest m modes. The other curves are obtained from Eq. (36) using the approximation Eq. (31) (dashed) and Eq. (47) (dash-dotted) for the form factor f_k . The thick dotted line labelled E_0 marks the energy of the ferromagnetic resonance given by Eq. (21); the thick dotted line labelled E_s is the energy $E_s = \hbar + \frac{1}{2}$ of the classical surface mode for $\Theta_k = 90$ at large wave-vectors, see Eqs. (22, 23).

where P_0 excludes the term $y_{ij} = z_{ij} = 0$ when $x_{ij} = 0$. As these sums are slowly converging and previously used summation techniques [22] are not very efficient for small wave-vectors needed for the dipolar-dominated spectrum of YIG, we use the Ewald summation technique to obtain fast convergence. Details of the calculation can be found in the appendix. To determine the dispersion of all m modes we numerically calculate the roots of Eq. (18) which can be easily done up to a film thickness $d = 7 \text{ \mu m}$. Using the fact that $\omega \sim 2.803 \cdot 10^3 \text{ GHz/Oe}$ we plot all results in units of GHz which is most convenient for experiments using microwave resonators and antennas to detect magnetic excitations. Typical magnon dispersions for different angles Θ_k between the propagation direction and the magnetic field are shown in Fig. 2 for a film with thickness $d = 400 \text{ \AA}$. Since our approach includes all effects of the exchange and the dipolar interaction within linear spin wave theory, it reproduces semiclassical approximations based on the Landau-Lifshitz equation at long wavelengths. In particular, for $k \neq 0$ the dispersion of the lowest m mode approaches, independently of the thickness d , the classical ferromagnetic resonance energy

$$E_0 = \frac{p}{h(h + \frac{1}{2})}; \quad (21)$$

where we introduced the characteristic magnon energy due to dipolar interactions,

$$p = 4 M_s: \quad (22)$$

The energy E_0 is indicated as a dotted line in Fig. 2. The spacing between different magnon modes decreases with increasing film thickness d ; for example in Fig. 3 we show the magnon spectrum of a film with thickness $d = 4040 \text{ \AA} = 5 \text{ \mu m}$, which forms already a quasi-

continuum for energies close to the ferromagnetic resonance. Moreover in the regime $dk \ll 1$ one observes that the energy of the n -th m mode deviates from the first m mode by an energy $E_n = \frac{1}{2} \omega_{ex}^2 n^2 = d^2$ which reflects the well known quadratic behaviour of ferromagnetic spin waves in three dimensions.

Of particular interest is the lowest magnon mode, whose dispersion is illustrated in Fig. 4. For propagation directions parallel to the magnetic field ($\Theta_k = 0$) we recover the well known [6] minimum of the lowest magnon mode at a finite wave-vector k_{min} where large magnon densities have been detected by their microwave radiance [1, 5]. As illustrated in Fig. 5, the position of the minimum depends on the film thickness as expected and is less pronounced for ultrathin films. With increasing propagation angle Θ_k the minimum becomes more shallow and completely disappears for $\Theta_k = 90$. From Figs. 2 and 3 it is also obvious that for angles $\Theta_k > 45$ the lowest modes shift upwards and tend to hybridize with higher modes. However, in the absence of additional symmetries the energy levels never cross. The magnon modes with finite group velocities $v_g(k) = \frac{1}{\hbar} \frac{\partial E_k}{\partial k}$ tend upwards and form the quasi-continuous surface mode. There are no further hybridizations as soon as the mode energies reach the energy

$$E_s = \hbar + \frac{1}{2} \quad (23)$$

of the classical surface mode.

3.2 Uniform mode approximation

The dispersion of the lowest magnon band can be derived from an effective in-plane Hamiltonian using various approximations. In fact, at long wavelengths the dispersion

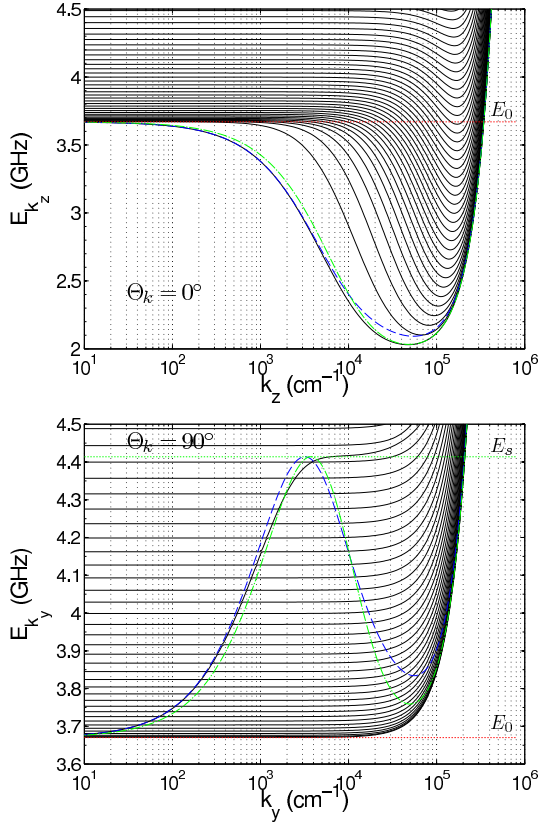


Fig. 3. (Color online) Spin-wave dispersion of a YIG film with thickness $d = 4040a = 5 \text{ nm}$ for wave-vectors parallel to the external field $H_e = 700 \text{ Oe}$ for $k_x = 0$ (top) and for $k_x = 90$ (bottom).

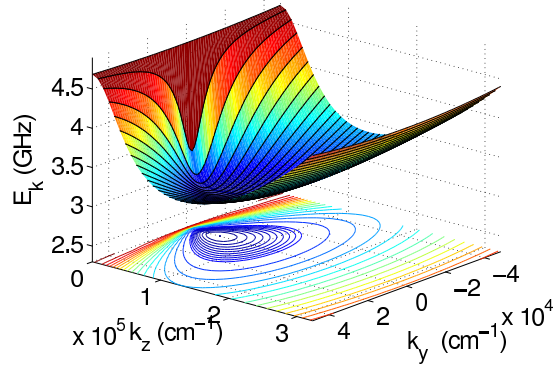


Fig. 4. (Color online) Spin-wave dispersion of the lowest mode of a YIG film with $H_e = 1000 \text{ Oe}$ and $d = 5.1 \text{ nm}$ obtained from the numerical solution of Eq. (18). Starting from the minimal energy E_{\min} contour lines with the spacing 20 MHz are shown to illustrate the rather flat minimum, whereas for larger energies the distance between contour lines is 100 MHz .

of the lowest magnon band can also be obtained within the microscopic approach based on the Landau-Lifshitz equation [6]. In the simplest approximation, we ignore the fact that the system is not translationally invariant in the x -direction and approximate the corresponding eigenfunctions by plane waves. The lowest magnon band is then

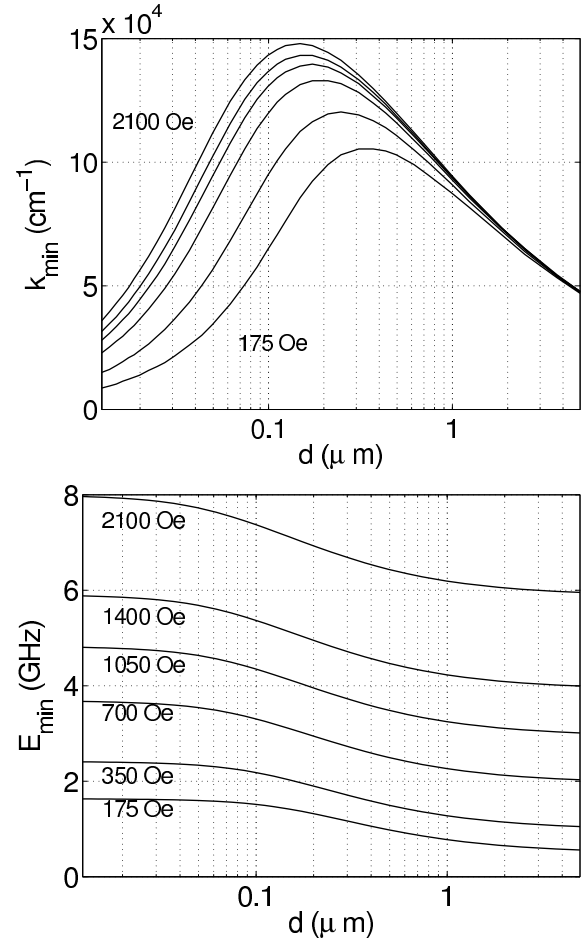


Fig. 5. Momentum k_{\min} and energy E_{\min} of the minimum in the dispersion of the lowest magnon mode for $k_x = 0$ as a function of film thickness for different magnetic fields. From top to bottom $H_e = 2100; 1400; 1050; 700; 350; 175 \text{ Oe}$.

obtained by replacing the operators $b_k(x_i)$ in Eq. (15) by

$$b_k(x_i) = \frac{1}{N} \sum_j b_k(x_j) e^{-\frac{1}{N} b_k} \quad (24)$$

Then Eq. (15) reduces to

$$\hat{H}_2^e = \sum_k A_k b_k^y b_k + \frac{B_k}{2} b_k b_k + \frac{B_k}{2} b_k^y b_k^y \quad ; \quad (25)$$

with

$$A_k = \frac{1}{N} \sum_{ij} A_k(x_{ij}) \quad ; \quad (26a)$$

$$B_k = \frac{1}{N} \sum_{ij} B_k(x_{ij}) \quad ; \quad (26b)$$

We parameterize the in-plane wave-vectors as

$$k = |k| (\cos \theta_k e_z + \sin \theta_k e_y) \quad ; \quad (27)$$

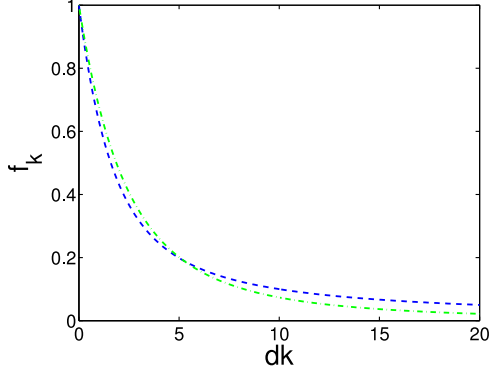


Fig. 6. (Color online) Plot of the form factors Eq. (31) for the uniform mode approximation (dashed) and Eq. (47) for the lowest eigenmode approximation (dash-dotted). For the samples used in the experiments the minimum of the lowest mode is at $dk \approx 5$ where the lowest eigenmode approximation is more accurate.

carry out the integrations over the two infinite directions and obtain for $\mathbf{x}_{ij} \notin 0$

$$D_k^{xx}(\mathbf{x}_{ij}) = D_k(\mathbf{x}_{ij}); \quad (28a)$$

$$D_k^{yy}(\mathbf{x}_{ij}) = \sin^2 k D_k(\mathbf{x}_{ij}); \quad (28b)$$

$$D_k^{zz}(\mathbf{x}_{ij}) = \cos^2 k D_k(\mathbf{x}_{ij}); \quad (28c)$$

$$D_k^{xy}(\mathbf{x}_{ij}) = \sin k D_k(\mathbf{x}_{ij}) \frac{\mathbf{j} \cdot \mathbf{j}}{x_{ij}} + \frac{\text{sign}(x_{ij})}{x_{ij}^2}; \quad (28d)$$

where

$$D_k(\mathbf{x}_{ij}) = \frac{2}{a^2} \mathbf{j} \cdot \mathbf{j} \mathbf{j} \cdot \mathbf{j} x_{ij} \mathbf{j}. \quad (29)$$

It should be noted that in the derivation of the dipolar tensor (28a-28d) we have implicitly assumed that $\mathbf{x}_{ij} \notin 0$. This has important consequences when we also replace the sum $\sum_{\mathbf{x}_i}$ by the integral $\int_{d=2}^{d=2} dx$. To properly account for the factor $(1 - \delta_{ij})$ in the dipole tensor in Eq. (7) we therefore exclude a sphere of infinitesimal radius around $x_{ij} = y_{ij} = z_{ij} = 0$ in our integrations, giving rise to the dipole matrix elements

$$D_k^{xx} = \frac{4}{a^3} \frac{h_1}{3} \mathbf{f}_k; \quad (30a)$$

$$D_k^{yy} = \frac{4}{a^3} \frac{h_1}{3} + \sin^2 k (\mathbf{f}_k - 1); \quad (30b)$$

$$D_k^{zz} = \frac{4}{a^3} \frac{h_1}{3} + \cos^2 k (\mathbf{f}_k - 1); \quad (30c)$$

and $D_k^{xy} = 0$. Here we have introduced the form factor [30]

$$\mathbf{f}_k = \frac{1}{\mathbf{j} \cdot \mathbf{j}} \frac{e^{\mathbf{j} \cdot \mathbf{j} i}}{\mathbf{j} \cdot \mathbf{j}} = 1 - \frac{\mathbf{j} \cdot \mathbf{j}}{2} + O(k^2 d^2); \quad (31)$$

which is shown as a dashed line in Fig. 6. From Eqs. (30a-30c) it is immediately obvious that our dipole elements satisfy the constraint

$$D_k^{xx} + D_k^{yy} + D_k^{zz} = 0; \quad (32)$$

which follows also directly from the definition (7) of the dipolar tensor. In terms of the above dipole matrix elements we can now write the coefficients A_k and B_k as

$$A_k = h + JS \left[4 - 2 \cos(k_y a) - 2 \cos(k_z a) \right] \frac{S}{2} D_k^{xx} + D_k^{yy} + \frac{1}{3}; \quad (33a)$$

$$B_k = \frac{S}{2} D_k^{xx} - D_k^{yy}; \quad (33b)$$

The magnon dispersion E_k is now obtained by diagonalizing the effective Hamiltonian (25) via a Bogoliubov transformation [15,16], resulting in

$$E_k = \frac{q}{A_k} \frac{p}{\mathcal{B}_k} \mathbf{j} = \frac{p}{(A_k - \mathcal{B}_k)(A_k + \mathcal{B}_k)}; \quad (34)$$

If we expand the terms involving the exchange interaction for small k (which is sufficient for the energy range in experiments on thin films) we get

$$JS \left[4 - 2 \cos(k_y a) - 2 \cos(k_z a) \right] \approx JS a^2 k^2 = \epsilon_x k^2; \quad (35)$$

We can then simplify the dispersion to

$$q E_k = \frac{\epsilon_x k^2}{[h + \epsilon_x k^2 + (1 - \mathbf{f}_k) \sin^2 k][h + \epsilon_x k^2 + \mathbf{f}_k]}; \quad (36)$$

which is indicated by dashed lines in Figs. 2, 3 and 7. Obviously, this approximation is in good qualitative agreement with the numerical result for the lowest mode as long as $k \lesssim 0.45$. Eq. (36) has been used in Ref. [30] to discuss the role of magnon-magnon interactions in YIG and has recently been rederived by Rezende [20]. Note, however, that in Fig. 3 one clearly sees deviations from the numerical result at intermediate wave-vectors in the interval $5 \lesssim \mathbf{j} \cdot \mathbf{j} \lesssim 50$. By comparing Fig. 2 with Fig. 3 we conclude that for the samples used in experiments [1,2,3,4,5,8,9,10,11] the minimum of the dispersion is exactly in this range so that better analytical approximations are needed for a more accurate description of the magnon dispersion in the vicinity of the minimum.

3.3 Lowest eigenmode approximation

To derive the dispersion of the lowest magnon mode more systematically, suppose that the $\mathbf{b}_k(\mathbf{x}_i)$ form (for fixed k) a complete set of orthogonal functions with respect to the x -direction, i.e.,

$$\int_{\mathbf{x}_i} \mathbf{b}_{nk}(\mathbf{x}_i) \mathbf{b}_{mk}(\mathbf{x}_i) = \delta_{nm}; \quad (37)$$

$$\int_{\mathbf{x}_i} \mathbf{b}_{nk}(\mathbf{x}_i) \mathbf{b}_{nk}(\mathbf{x}_j) = \delta_{ij}; \quad (38)$$

We may then expand the operators $b_k(\mathbf{x}_i)$ in this basis,

$$b_k(\mathbf{x}_i) = \sum_n \mathbf{b}_{nk}(\mathbf{x}_i) b_{nk}; \quad (39)$$

where

$$b_{nk} = \sum_{x_i} \sum_{n_k} (x_i) b_k(x_i); \quad (40)$$

Let us retain in the expansion (39) only the $n = 0$ term,

$$b_k(x_i) \approx b_{0k}(x_i) b_{0k}; \quad (41)$$

If we choose $b_{0k}(x_i) = \frac{1}{\sqrt{N}}$ (corresponding to the $n = 0$ term in the plane wave expansion) and identify $b_k \approx b_{0k}$ we recover Eq. (24). However, a truncated expansion in plane waves seems not to be a good approximation for a system of finite width. To improve on the approximation (24) it is better to expand in terms of the eigenfunctions of the exchange matrix given in Eq. (17),

$$\sum_{x_j} J_k(x_{ij}) \sum_{n_k} (x_j) = \sum_{n_k} J_{nk}(x_i); \quad (42)$$

For open boundary conditions these are standing waves with nodes at $x = d/2, \text{ i.e.,}$

$$\sum_{n_k} (x_i) = \frac{1}{\sqrt{N}} \sin[k_n(x_i + d/2)]; \quad (43)$$

where $k_n = (n + 1)\pi/d, n = 0; 1; \dots; N - 1$. The approximation (41) then reduces to

$$b_k(x_i) \approx \frac{1}{\sqrt{N}} \cos(k_0 x_i) b_k; \quad (44)$$

with $k_0 = \pi/d$, and

$$b_k = \sum_{x_i} \frac{1}{\sqrt{N}} \cos(k_0 x_i) b_k(x_i); \quad (45)$$

Substituting Eq. (44) into Eq. (15) we obtain again an effective Hamiltonian of the form (25), but now with

$$A_k = \frac{2}{N} \sum_{ij} \cos(k_0 x_i) \cos(k_0 x_j) A_k(x_{ij}); \quad (46a)$$

$$B_k = \frac{2}{N} \sum_{ij} \cos(k_0 x_i) \cos(k_0 x_j) B_k(x_{ij}); \quad (46b)$$

Again the summations are replaced by integrations which can be carried out analytically and result in the dispersion of the form of Eq. (36), but with the form factor now given by

$$\begin{aligned} f_k &= 1 - \frac{\sum_j k_d j^3 + \sum_j k_d j^2 + 2 \sum_j^2 (1 + e^{-k_d j})}{(k^2 d^2 + \sum_j^2)^2} \\ &= 1 - \frac{4}{2} \sum_j j l + O(k^2 d^2); \end{aligned} \quad (47)$$

In Fig. 6 we compare this form factor with the corresponding form factor (31) obtained within the uniform mode approximation. Obviously, there are only small differences: the linear coefficient in the Taylor series is different, resulting in a smaller slope of the dispersion (36) at $k = 0$.

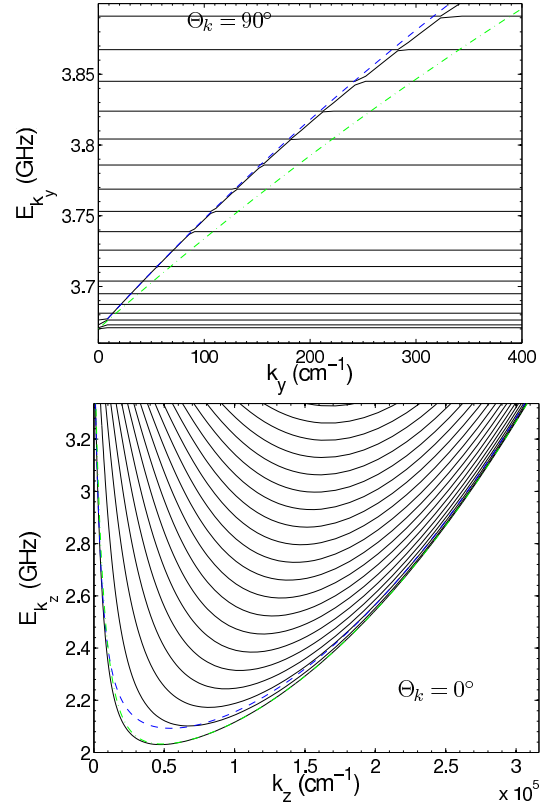


Fig. 7. (Color online) Enlarged details of Fig. 3 on a linear momentum scale: spin-wave dispersion of a YIG film with thickness $d = 4040a = 5 \text{ nm}$ for wave-vectors parallel to the external magnetic field $H_e = 700 \text{ Oe}$ ($k_x = 0$, top) and for wave-vectors perpendicular to the magnetic field ($k_x = 90^\circ$, bottom). The solid lines are exact numerical results obtained from the solution of Eq. (18). The dashed line is our approximate expression (36) for the lowest magnon band, using the uniform mode approximation (31) for the form factor. The dashed-dotted line is the lowest magnon band with form factor (47) given by the lowest eigenmode approximation.

To estimate the validity of these approximations, we compare them in Figs. 7 and 8 with our numerically exact results of the model (2) for experimentally relevant parameters. In Fig. 7 we show the relevant details of Fig. 3 on a linear momentum scale; obviously for sufficiently large wave-vectors the lowest eigenmode approximation is more accurate and practically lies on top of the numerically exact result. On the other hand, for small wave-vectors the uniform mode approximation fits better, as illustrated by the lower part of Fig. 7. A more quantitative comparison between these two approximations for wave-vectors parallel to the magnetic field and different film thickness is shown in Fig. 8. Roughly, for $d \ll j \cdot 5$ the uniform mode approximation fits better, while for $d \gg j \cdot 5$ the lowest eigenmode approximation gives a better agreement with the numerical results. As there are not many states at small wave-vectors, we believe that the lowest eigenmode approximation is more suitable for a quantitative description of the magnon dispersion, in particular if one is interested in physical effects related to the dispersion minimum

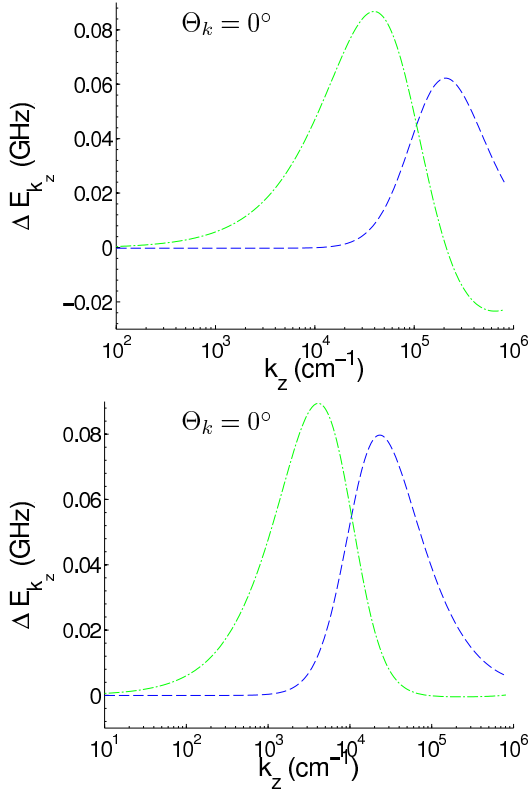


Fig. 8. (Color online) Accuracy of our two analytical approximations for the lowest magnon mode for a YIG film with $N = 400$ layers (top) and $N = 4040$ layers (bottom). Dashed line: difference between the numerical result and the uniform mode approximation; dash-dotted line: difference between the numerical result and the lowest eigenmode approximation.

at $k_{m \text{ in}}$. On the other hand, both analytical approximations describe the quasi-continuous surface mode for large $k_z > 45$ rather accurately as long as the wave-vectors are sufficiently small so that the dispersion curves tend upwards due to the presence of exchange interaction [7] and hybridize.

4 Conclusions and outlook

In this work we have presented a comprehensive discussion of the spin-wave spectra of experimentally relevant samples of thin films of the magnetic insulator YIG. Starting from an effective spin- S Heisenberg Hamiltonian with exchange and dipole-dipole interactions on a cubic lattice, we have used a truncated Holstein-Primakoff transformation to obtain an effective quadratic boson Hamiltonian whose eigen-energies can be identified with the magnon energies. We have then used numerical methods to calculate the magnon dispersions for experimentally relevant films with thickness corresponding to a few thousand lattice spacings without further approximations. In order to carry out the dipolar sums entering the secular determinant, the use of efficient Ewald summation techniques was necessary. We have also estimated the accuracy of two different analytical approximations for the lowest magnon

band: the uniform mode approximation (where the transverse spatial variation of the eigenmodes is ignored) and the lowest eigenmode approximation (where the lowest transverse mode is approximated by the lowest eigenmode of the exchange matrix). For realistic films, the latter approximation is more accurate for wave-vectors in the vicinity of the dispersion minimum.

In contrast to the phenomenological approach based on the Landau-Lifshitz equation [6,7], in our microscopic approach it is straightforward to systematically take into account interaction effects. In future work we shall carefully derive the momentum-dependent interaction vertices of the bosonized effective in-plane Hamiltonian using the lowest eigenmode approximation, which according to our investigations in Sec. 3 is more accurate in the experimentally interesting regime of wave-vectors close to $k_{m \text{ in}}$. Although rough estimates of the interactions vertices can be found in the literature [30], more accurate microscopic calculations which properly take into account the momentum-dependence of the vertices are needed in order to gain a better understanding of the role of spin-wave interactions in the experiments [1,2,3,4,5,8,9,10,11]. For example, it would be interesting to know the intrinsic damping of the lowest magnon mode for wave-vectors close to $k_{m \text{ in}}$ due to magnon-magnon interactions.

We would like to thank A. A. Serga, T. Neumann and P. Pricozia for helpful discussions and gratefully acknowledge financial support by the SFB/TRR 49 and the DAAD/PROBRAL-program.

APPENDIX: DIPOLAR SUMS

For the calculation of the slowly converging sums in Eq. (20) we introduce the quantity

$$I_{\mathbf{k}}(\mathbf{x}_{ij}) = \sum_{y_{ij}, z_{ij}} \frac{e^{i(k_y y_{ij} + k_z z_{ij})}}{(\mathbf{x}_{ij}^2 + y_{ij}^2 + z_{ij}^2)^{5/2}}; \quad (\text{A } 1)$$

and get the dipolar sums as derivatives,

$$D_{\mathbf{k}}^{yy}(\mathbf{x}_{ij}) = \frac{\partial^2}{\partial k_z^2} \frac{2 \partial^2}{\partial k_y^2} \mathbf{x}_{ij}^2 I_{\mathbf{k}}(\mathbf{x}_{ij}); \quad (\text{A } 2a)$$

$$D_{\mathbf{k}}^{zz}(\mathbf{x}_{ij}) = \frac{\partial^2}{\partial k_y^2} \frac{2 \partial^2}{\partial k_z^2} \mathbf{x}_{ij}^2 I_{\mathbf{k}}(\mathbf{x}_{ij}); \quad (\text{A } 2b)$$

$$D_{\mathbf{k}}^{xx}(\mathbf{x}_{ij}) = \frac{\partial^2}{\partial k_y^2} + \frac{\partial^2}{\partial k_z^2} + 2\mathbf{x}_{ij}^2 I_{\mathbf{k}}(\mathbf{x}_{ij}); \quad (\text{A } 2c)$$

$$D_{\mathbf{k}}^{xy}(\mathbf{x}_{ij}) = i 3\mathbf{x}_{ij} \frac{\partial}{\partial k_y} I_{\mathbf{k}}(\mathbf{x}_{ij}); \quad (\text{A } 2d)$$

Note the symmetry $D_{\mathbf{k}}^{xx} = D_{\mathbf{k}}^{xx}$ and the relation $D_{\mathbf{k}}^{yy} = D_{\mathbf{k}}^{zz}$ with $\mathbf{k} = k_z \mathbf{e}_y + k_y \mathbf{e}_z$. To evaluate the above expressions, we consider the cases $\mathbf{x}_{ij} \neq 0$ and $\mathbf{x}_{ij} = 0$ separately.

A Case $x_{ij} \neq 0$

Using the identity

$$\int_0^Z x^{n-1} e^{-x} dx = \Gamma(n) - \int_0^Z (n-1)! e^{-x} dx \quad (A.3)$$

where $n > 0$; $\text{Re } \mu > 0$, and introducing the dummy variable μ to check the results, we can rewrite

$$I_k(x_{ij}) = \frac{4}{3} \int_0^Z dt t^{3-2} e^{-x_{ij}^2 t} e^{i(k_y y_{ij} + k_z z_{ij})} \quad (A.4)$$

We split the integral in two parts and use Ewald's method [24,31]

$$\int_0^Z e^{-\mu t} e^{ikr} = \frac{1}{a^2 \mu^2} \int_0^Z e^{-\frac{ik+g_j^2}{4\mu t}} \quad (A.5)$$

to transform the lattice sum into a lattice sum in reciprocal space, where $g = g_y e_y + g_z e_z$ is a reciprocal lattice vector. This yields

$$I_k(x_{ij}) = \frac{4}{3} \int_0^Z dt t^{1-2} e^{-\frac{ik+g_j^2}{4\mu t} x_{ij}^2 t} + \frac{1}{a^2 \mu^2} \int_0^Z dt t^{1-2} e^{-\frac{ik+g_j^2}{4\mu t} x_{ij}^2 t} \quad (A.6)$$

where

$$Ei(z) = \int_0^Z dt t e^{-zt} \quad (A.7)$$

is the Misra function,¹ which for $\mu = 3=2$ and $z = x > 0$ can also be written as

$$Ei(x) = e^{-x} \left(\frac{3+2x}{2x^2} + \frac{3^{p-1} Ei(\frac{x}{3})}{4x^{5-2}} \right) \quad (A.8)$$

Evaluating the integral in Eq. (A.6) for $p > 0$ and $q^2 > 0$ using

$$\int_0^Z dt t^{1-2} e^{-q^2 t} e^{-p^2 t} = \frac{e^{-p^2 q^2}}{q^2} + \frac{1}{4q^3} e^{-2pq} (1+2pq) Ei(p-q) + e^{-2pq} (1+2pq) Ei(p+q) \quad (A.9)$$

we can calculate the derivatives according to Eqs. (A.2) and finally get the result for the sums of the dipole interactions between spins located in different atomic layers,

¹ The Misra function is defined in terms of the exponential integral $Ei(z) = \int_1^z dx e^{-x} x^{-1}$ via $Ei(z) = Ei(z)$.

$$D_k^{xx}(x_{ij}) = \frac{2}{a^2} \sum_g \int_0^Z dt t^{1-2} e^{-p^2 t} e^{-q^2 t} (k_x + g_x) f(p; q) + \frac{4}{3} \sum_g \int_0^Z dt t^{1-2} e^{-p^2 t} e^{-q^2 t} (k_y^2 + 3k_z^2) \cos(k_y y_{ij}) \cos(k_z z_{ij}) Ei(\frac{x_{ij}^2}{3}) \quad (A.10a)$$

$$D_k^{yy}(x_{ij}) = \frac{2}{a^2} \sum_g \int_0^Z dt t^{1-2} e^{-p^2 t} e^{-q^2 t} \frac{(k_y + g_y)^2}{k_x + g_x} f(p; q) + \frac{4}{3} \sum_g \int_0^Z dt t^{1-2} e^{-p^2 t} e^{-q^2 t} (k_y^2 + 3k_z^2) \cos(k_y y_{ij}) \cos(k_z z_{ij}) Ei(\frac{x_{ij}^2}{3}) \quad (A.10b)$$

$$D_k^{xy}(x_{ij}) = i \frac{2}{a^2} \sum_g \int_0^Z dt t^{1-2} e^{-p^2 t} e^{-q^2 t} (k_y + g_y) f(p; q) + i \frac{4}{3} \sum_g \int_0^Z dt t^{1-2} e^{-p^2 t} e^{-q^2 t} x_{ij} y_{ij} \sin(k_y y_{ij}) \cos(k_z z_{ij}) Ei(\frac{x_{ij}^2}{3}) \quad (A.10c)$$

where we have used the abbreviations $q = \sqrt{x_{ij}^2}$ and $p = k_x + g_x (2^{-1})$ and have introduced the function

$$f(p; q) = e^{-2pq} Ei(p-q) + e^{2pq} Ei(p+q) \quad (A.11)$$

For the simple cubic lattice the components of the reciprocal lattice vectors are $g_y = 2\pi/m$; $g_z = 2\pi/n$; $g_x = 2\pi/l$. Note that this result is independent of the variable μ which shifts the weight from the sum s in real space to the sum s in reciprocal space as $\mu \rightarrow 0$ and therefore simplifies to the sums given in Ref. [22] for $\mu = 0$.

B Case $x_{ij} = 0$

In this case we have to exclude the point $r = 0$ because there is no self interaction. We therefore introduce the dummy variable $x = y e_y + z e_z$,

$$I_k(x_{ij} = 0) = I_k = \sum_r \frac{e^{ikr}}{r^5} \quad (A.12)$$

Using Eq. (A.3) we can rewrite Eq. (A.12) and use the transformation on the reciprocal lattice

$$\sum_r e^{ikr} \frac{1}{r^5} = \sum_g \int_0^Z dt t^{1-2} e^{-i(g+k)x} e^{-\frac{y^2+z^2}{4\mu t}} \quad (A.13)$$

We subtract $1 = \sum_r \frac{1}{r^5}$ from the sum on the left, which is equivalent to removing this first term in the sum over r in our dipole sum. In the limit $x \rightarrow 0$ we obtain,

$$I_k = \frac{8}{9a^2} \sum_g \int_0^Z dt t^{1-2} e^{-p^2 t} (1 - p^2) + 2 \sum_g \int_0^Z dt t^{1-2} e^{-p^2 t} p^3 Ei(p) + \frac{8}{9} \sum_g \int_0^Z dt t^{1-2} e^{-p^2 t} (1 - 2r^2) + 2 \sum_g \int_0^Z dt t^{1-2} e^{-p^2 t} Ei(\frac{x_{ij}^2}{3}) \quad (A.14)$$

After taking the derivatives according Eq. (A.2) we note that we get for the dipolar sums the limit $q = x_{ji} \rightarrow 0$ of Eq. (A.10) and therefore the removing of the origin does not make any difference in the calculation of the dipolar sums except for omitting the term $r = 0$ in the real space sums.

References

1. S. O. Demokritov, V. E. Demidov, O. Dzyapko, G. A. Melkov, A. A. Serga, B. Hillebrands, and A. N. Slavin, *Nature* 443, 430 (2006)
2. V. E. Demidov, O. Dzyapko, S. O. Demokritov, G. A. Melkov, and A. N. Slavin, *Phys. Rev. Lett.* 99, 037205 (2007)
3. O. Dzyapko, V. E. Demidov, S. O. Demokritov, G. A. Melkov, and A. N. Slavin, *New J. Phys.* 9, 64 (2007)
4. V. E. Demidov, O. Dzyapko, S. O. Demokritov, G. A. Melkov, and A. N. Slavin, *Phys. Rev. Lett.* 100, 047205 (2008)
5. S. O. Demokritov, V. E. Demidov, O. Dzyapko, G. A. Melkov, and A. N. Slavin, *New J. Phys.* 10, 045029 (2008)
6. B. A. Kalinikos and A. N. Slavin, *J. Phys. C: Solid State Phys.* 19, 7013 (1986)
7. M. G. Cottam, editor, *Linear and Nonlinear Spin Waves in Magnetic Films and Superlattices*, World Scientific, Singapore (1994)
8. A. A. Serga, A. V. Chumak, A. Andre, G. A. Melkov, A. N. Slavin, S. O. Demokritov, and B. Hillebrands, *Phys. Rev. Lett.* 99, 227202 (2007)
9. S. Schafer, A. V. Chumak, A. A. Serga, G. A. Melkov, and B. Hillebrands, *Appl. Phys. Lett.* 92, 162514 (2008)
10. A. V. Chumak, A. A. Serga, B. Hillebrands, G. A. Melkov, V. Tiberkevich, and A. N. Slavin, *Phys. Rev. B* 79, 014405 (2009)
11. T. Neumann, A. A. Serga, and B. Hillebrands, *Appl. Phys. Lett.* 93, 252501 (2008)
12. T. Holstein and H. Primako, *Phys. Rev.* 58, 1098 (1940)
13. F. J. Dyson, *Phys. Rev.* 102, 1217, 1230 (1956)
14. S. M. Aliev, *Zh. Eksper. Teor. Fiz.* 33, 1010 (1957)
15. A. I. Akhiezer, V. G. Bar'yakhtar, and S. V. Peletminskii, *Spin Waves*, North Holland, Amsterdam (1968)
16. D. C. Mattis, *The theory of magnetism made simple*, World Scientific, Singapore (2006)
17. R. P. Erickson and D. L. Mills, *Phys. Rev. B* 43, 10715 (1991)
18. R. P. Erickson and D. L. Mills, *Phys. Rev. B* 44, 11825 (1991)
19. J. J. M. Pereira and M. G. Cottam, *J. Appl. Phys.* 85, 4949 (1999)
20. S. M. Rezende, *Phys. Rev. B* 79, 174411 (2009)
21. R. N. Costa Filho, M. G. Cottam, and G. A. Farias, *Solid State Commun.* 108, 439 (1998)
22. R. N. Costa Filho, M. G. Cottam, and G. A. Farias, *Phys. Rev. B* 62, 6545 (2000)
23. H. Benson and D. L. Mills, *Phys. Rev.* 178, 839 (1969)
24. J. M. Ziman, *Principles of the Theory of Solids*, Cambridge University Press, Cambridge (1979)
25. M. P. Kostylev, G. Gubbiotti, J.-G. Hu, G. Carlotti, T. Ono, and R. L. Stamps, *Phys. Rev. B* 76, 054422 (2007)
26. V. Cherepanov, I. Kolkolov, and V. L'vov, *Physics Reports* 229, 81 (1993)
27. M. A. Gilio and S. Geller, *Phys. Rev.* 110, 73 (1958)
28. B. R. Titman, *Solid State Commun.* 13, 463 (1973)
29. A. G. Gurevich and G. A. Melkov, *Magnetization Oscillations and Waves*, CRC Press, Boca Raton (1996)
30. I. S. Tupitsyn, P. C. E. Stamp, and A. L. Burin, *Phys. Rev. Lett.* 100, 257202 (2008)
31. L. Bartosch, L. Balents, and S. Sachdev, *Ann. Phys. (New York)* 321, 1528 (2006)